INTERNATIONAL JOURNAL FOR NUMERICAL METHODS IN FLUIDS, VOL. 20, 469–492 (1995)

MODELLING OF THE TURBULENT THERMAL BOUNDARY LAYER IMPLEMENTED IN CFD CODE N3S AND APPLICATION TO FLOWS IN HEATED AND COOLED ROOMS

B. DELENNE AND D. MANZONI

Department TTA, EDF/DER, 6 quai Watier, 78400 CHATOU CEDEX France

G. POT

Department LNH, EDF/DER, 6 quai Watier, 78400 CHATOU CEDEX, France

SUMMARY

This paper presents an efficient finite element method for solving the unsteady Navier–Stokes equations for turbulent incompressible flow coupled with thermal problems. This method has been implemented in the N3S code, developed at Electricité de France. The time discretization is first described. We precise then the Chorin and the 'projected Uzawa' algorithms used for the Stokes problem. Recent improvements concerning the optimization of finite element calculations are also detailed. The second part deals with the modelling of the thermal boundary layer used to simulate walls with fixed temperature in turbulent flows. The differences with other modelling suggested in the literature are discussed. The last part presents some applications. EDF is involved in the conception of heating or cooling systems and numerical methods constitute a very useful tool to study the movements of air in habitations. The calculations are validated by comparisons with measurements.

KEY WORDS: boundary layer; heat transfer; turbulence; CFD; finite elements

1. INTRODUCTION

Air movements in heated or cooled rooms raise a great challenge for numerical methods. A finite element approach is suggested in this paper to solve the Navier–Stokes equations coupled with buoyancy forces. The turbulent effects, quite important for the representation of the heat transfer, are taken into account with a classical k–ε model. Four typical configurations of mixed convection flows in enclosures representative of ventilation and heating problems were computed. Bidimensional simulations have been successfully compared with experimental results: the velocity sfield simulated is in good agreement with experiments, a slightly less accuracy on the temperature field has been noticed for particular configurations. An appropriate modelling of the turbulent thermal boundary layer is expected. The formulation adopted, based on a classical wall laws, is presented in the first part of this paper.

This study has been achieved to qualify the finite element (FE) code N3S developed by the 'Direction des Etudes et Recherches' of Electricité de France for simulating turbulent incompressible[1] and dilatable[2] flows. N3S is nowadays used for many industrial applications (internal flows[1], thermal problems[3], turbomachinery[4]). These applications are more and more important (calculation until 370 000 nodes and 1 800 000 unknowns), so an important work has been done to

CCC 0271–2091/95/060469–24

Received 3 February 1994
Revised 2 November 1994

improve the release 3·1 of the code in terms of CPU time and memory allocation on super computers as CRAY Y-MP. A specific algorithm has also been developed to solve the Stokes problem in such different configurations: the projected Uzawa/Chorin algorithm.

2. MODELLING OF THE THERMAL BOUNDARY LAYER

2.1. The boundary conditions

The flows studied with thermohydraulic codes are usually bounded by walls. The modelling of the turbulence and the heat transfer in the vicinity of these walls is quite difficult. Many solutions are suggested in the literature. The turbulent effects in the core of the flow are taken into account in N3S by a k–ε model and the different solutions to simulate the turbulent boundary layer can be divided into two groups. First, the most sophisticated methods, like the low-Reynolds models,[5] compute all the gradients in the boundary layer considering the physically correct no slip condition. These methods are the most accurate but require very thin meshes in the wall area and the number of nodes becomes quickly far too high for industrial calculations. The other classical ways to simulate the boundary layers are the *wall laws*,[6–8] that is, rather than apply the no slip condition at the wall, the modelling of the turbulent boundary layer supply the shear stress $\tau_w(\tau_w = \rho u_*^2)$ at a given distance from the wall $\delta_0(\delta_0$ is small compared to the characteristic size of the mesh at the wall). So as far as the finite element discretization is concerned, the numerical boundary is not actually on the wall but fictitiously shifted inside the domain at the distance δ_0 where the shear stresses are evaluated. This method does not require any great refinement in the wall area.

On a thermal point of view, different kinds of boundary conditions could be used in N3S, such as Dirichlet conditions in inlet, Neumann conditions on heating or cooling walls. As an analogy with the momentum transfer, walls that are kept at fixed temperature raise many problems in turbulent flows, and one more time, instead of applying numerically the continuity of the temperature profile at the wall, the modelling of the thermal boundary layer evaluates the heat flux from wall to fluid. Many models can be found, the simplest ones, based on Prandtl–Taylor analogy, consider that viscous and thermal sublayers are of the same order of magnitude. The main disadvantage of these proceedings is that the very small, or, on the opposite, very high Prandtl number (Pr) fluids cannot be taken into account. The formulation that was chosen is the one suggested by Arpaci and Larsen.[9]

2.2 The modelling of the thermal boundary layer for $Pr \ll 1$

Considering a steady flow on a plate kept at fixed temperature T_w, the heat flux (q_w) from the plate can be written as

$$q_w = \rho C_p (a + a_t) \frac{dT}{dy} \tag{1}$$

on a dimensionless form:

$$1 = a_e^+ \frac{dT^+}{dy^+} \tag{2}$$

The purpose of the model is to describe with precision the diffusivity parameter a_e^+. On a first approach, the boundary layer can be divided into two parts, one near the wall dominated by the

molecular diffusion, the other by the turbulent diffusion. In the first region, the turbulent terms can be neglected and the equivalent diffusivity is reduced to

$$a_e^+ = \frac{a}{v} = \frac{1}{Pr} \tag{3}$$

On the opposite, in the second region, the heat transfer is mainly due to turbulent diffusion. The parameter a_t is simply related to the eddy viscosity v_t through the turbulent Prandtl number concept. The turbulent Prandtl number (Pr_t) is supposed to be constant. The expression of the eddy viscosity is given by the mixing length model applied in the core of the boundary layer where the logarithmic velocity distribution is valid:

$$v_t = (l_m^+)^2 \left| \frac{\partial U^+}{\partial y^+} \right| = v\kappa y^+ \Rightarrow a_e^+ = \frac{\kappa y^+}{Pr_t} \tag{4}$$

Those two regions in the boundary layer are not necessarily separated. Considering fluids for which the conductivity is high enough, the molecular diffusion contributes to the heat transfer in the turbulent region, that is, the conduction sublayer is thicker than the viscous one. For this kind of fluids, clearly small Prandtl number fluids, the equations (3) and (4) intersect and the temperature distribution for $Pr \ll 1$ can be described by

$$y^+ \leqslant \frac{Pr_t}{k\,Pr} = y_0^+ : \quad a_e^+ = \frac{1}{Pr} \Rightarrow T^+ = Pry^+ \tag{5a}$$

$$y^+ > \frac{Pr_t}{\kappa\,Pr} = y_0^+ : \quad a_e^+ = \frac{\kappa y^+}{Pr_t} \Rightarrow T^+ = \frac{Pr_t}{\kappa}\left(Ln\left(\frac{\kappa Pr}{Pr_t} y^+ \right) + 1 \right) \tag{5b}$$

The dimensionless thickness of the conduction layer: y_0^+ and the integration constant are determined by assuming that the equivalent diffusivity and the temperature are continuous.

2.3. *The modelling of the thermal boundary layer for* $Pr \geqslant 1$

A modelling of the thermal boundary layer that consider only very small Prandtl number fluids is not satisfying That would mean that only liquid metal flows can be simulated by the code, and that the model cannot be applied to oil ($Pr > 100$), water ($Pr \approx 10$) or even gases ($Pr = 0{\cdot}7$ for the air). For those fluids, the near-wall thermal sublayer is immersed in the viscous sublayer. This suggests to introduce a third intermediate layer between the molecular and the logarithmic regions in which the heat transfer is determined not only by conduction but also by turbulent diffusion. The mixing length theory cannot be applied crudely because the flow in this part of the boundary layer is not fully turbulent. Arpaci and Larsen retain Levitch's suggestion which is

$$v_t/v \approx (y^+)^3 \tag{6}$$

This formulation is in good agreement with Van Driest[6] who developed an expression for the mixing length all over the boundary layer. So, in this third layer, the equivalent diffusivity is

$$a_e^+ = \frac{1}{Pr} + \frac{a_1}{Pr_t}(y^+)^3 \tag{7}$$

Kader and Yaglom[7] expected from experimental results the relation

$$a_1/Pr_t = 10^{-3} \tag{8}$$

These considerations lead to the following equations for $Pr \geqslant 1$:

$0 < y^+ \leqslant y_1^+$

$$a_e^+ = \frac{1}{Pr} \Rightarrow T^+ = Pr\, y^+ \tag{9a}$$

$y_1^+ < y^+ \leqslant y_2^+$

$$a_e^+ = \frac{1}{Pr} + \frac{a_1}{Pr_t}(y^+)^3 \Rightarrow T^+ = \frac{1}{3}ab^{-2/3}\left[\mathrm{Ln}(y^+ + b^{1/3}) - \frac{1}{2}\mathrm{Ln}(y^{+2} - b^{1/3}y^+ + b^{2/3}) + \sqrt{3}\,\mathrm{Arctg}\left(\frac{2y^+}{\sqrt{3}b^{1/3}} - \frac{1}{\sqrt{3}}\right)\right] + c_1 \tag{9b}$$

$y_2^+ < y^+$

$$a_e^+ = \frac{1}{Pr} + \frac{\kappa y^+}{Pr_t} \Rightarrow T^+ = \frac{Pr_t}{\kappa}\mathrm{Ln}\left(\frac{Pr_t}{Pr\,\kappa} + y^+\right) + c_2 \tag{9c}$$

with

$$a = Pr_t/a_1 \quad \text{and} \quad b = a/Pr$$

This set of equations is a bit different from the one derived by Arpaci and Larsen[9] who neglected the molecular terms not only in the outer part of the boundary layer but also in the intermediate zone. So the present formulation is more complex but it is supposed to be more accurate in the description of the temperature profiles especially for high Prandtl numbers fluids. The determination of the thickness and of the constants require a special attention. They cannot be obtained simply by writing the continuity of the temperature and of equivalent diffusivity.

In a first approach, the expression in the medium region (9b) was supposed to be appropriate to represent the heat transfer down to the wall. As a matter of fact, the equation suggests that the dimensionless temperature is linear for the smallest values of y^+. This assumption led to a set of only two equations one for the outer part of the boundary layer, the second covering the intermediate and the near-wall area. But this has never been implemented in the code, the comparisons (Figure 1) with the measurements reported in Kader's review[8] indicate that the heat flux is under-estimated.

In the first approach, the higher accuracy of the model did not improve the solution and the separation into three different regions seems to be essential. The formulation chosen, retain one pure conduction region as written in equations (9). According to dimensional arguments, the thickness of the thermal conduction sublayer y_1^+ can be determined by equating the molecular terms to the turbulent ones:

$$\frac{1}{Pr} = \frac{a_1}{Pr_t}(y_1^+)^3$$

The continuity of the temperature all over the boundary layer and the continuity of the equivalent diffusivity at the boundary between the intermediate and logarithmic layers supply the thickness y_2^+ of the intermediate zone and the two integration constants c_1 and c_2. In this formulation, the expression of the equivalent diffusivity is not continued at the end of the conduction sublayer, but this has no consequence, for $Pr \geqslant 1$ the conduction layer is of the same order of magnitude than the viscous sublayer so very thin in fully turbulent flows and the deviation induced on the dimensionless temperature suits the measurements (Figure 1). It must be

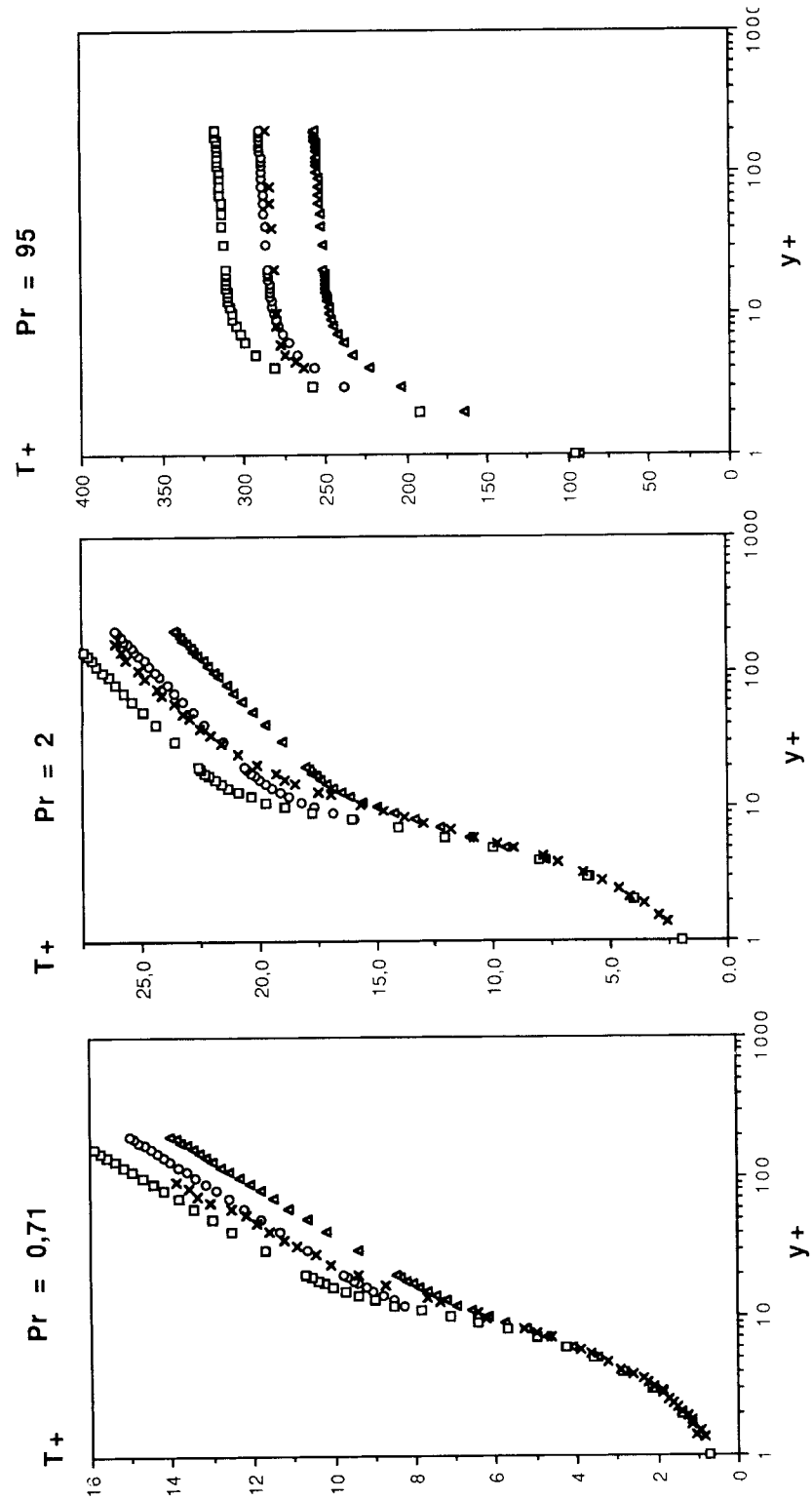

Figure 1. Profiles of dimensionless temperature for different Prandtl numbers.

emphasised that the dimensionless temperature profile depends only on the property of the fluid (i.e. the Prandtl number) and on the dimensionless distance to the wall. This model has been validated by comparisons with thermal measurements from the literature, one application is reported in Reference 3.

3. GENERAL PRESENTATION OF THE NUMERICAL METHODS

3.1. Presentation of the problem

The equations governing the fluid motion in a regular open bounded subset Ω of $\mathbf{R}^N$ (N = 2 or 3) and over a time interval $[0, t]$ are the Navier–Stokes equations for velocity $\mathbf{v}$ and pressure p. For some flows of the thermal convection type, we assume that density variations with temperature T are small enough to be taken into account with the Boussinesq approximation. The energy equation gives the evolution of the temperature T which satisfies a convection diffusion equation. It is also possible to take into account more important thermal effects which lead to consider the Navier–Stokes problem with varying density ρ. This modelling is operational in the code today.

Industrial flows computed with N3S code are generally turbulent and characterized by very high Reynolds numbers. To simulate such complex non-linear flows, we consider the average value of physical quantities (velocity, pressure and temperature if necessary) which we calculate by means of a model for correlations between fluctuating velocities and between velocity and temperature fluctuations. The model used[10] or k–ε model is made up of two equations in which k denotes the turbulent kinetic energy and ε the turbulent dissipation rate.

3.2. Boundary conditions

Boundary conditions depend on the type of boundary which is to be dealt with. At the inlet Γ_{in} of the Ω fluid domain, forced constrained conditions (Dirichlet) are used for all the variables. At the outlet Γ_{out} of the Ω fluid domain, vanishing normal stress for the velocity and vanishing flux conditions (homogeneous Neumann) for scalar quantities are used. For walls Γ_w a modelling based on the generalization of the analysis of the boundary layer on a flat plate is used. For velocity, the normal component satisfies an impermeability condition ($\mathbf{v} \cdot \mathbf{n} = 0$, where $\mathbf{n}$ is the normal exterior to the wall). This condition is completed by a friction condition on the tangential stress. We furthermore assume that near the wall, there is an equilibrium between turbulent production and dissipation which enables to express k and ε at the wall. Flux conditions are imposed for temperature θ. To sum up, wall boundary conditions on scalar quantities T, k and ε are either of Dirichlet type (for k and ε) or of Neumann type (for T).

3.3. Time discretization

Time discretization of scalar equations of convection diffusion as well as the Navier–Stokes equations is realized thanks to a fractional step scheme. The convection step is processed by a characteristics method and the diffusion or Stokes step thanks to an implicit Euler scheme.

Convection step. The kth-order characteristics scheme consists in computing an approximation at time t^{n+1} in $[0, t]$ of the total derivative of any scalar quantity C (or the velocity $\mathbf{v}$) with the help of a kth-order backward differentiation scheme integrated along the characteristics curve defined on the time interval $[t^{n-k+1}, t^{n+1}]$.

Diffusion or Stokes step. We can now compute C^{n+1} ($\mathbf{v}^{n+1}$ and p^{n+1}) which denotes an approximation at time t^{n+1} by solving a diffusion problem (or a Stokes problem for velocity $\mathbf{v}$ and pressure p) by a classical kth-order backward differentiation scheme.

A theoretical analysis of the whole scheme has been done.[11] In N3S code, the 1st-order and 2nd-order schemes have been implemented.

3.4. *Space discretization and Stokes problem with varying density*

For the generalized Stokes problem, the classical continuity equation becomes: $\nabla \cdot \rho \mathbf{v} = 0$. It can be theoretically shown that this problem is well posed,[12] for two types of formulation (velocity–pressure or momentum: $\mathbf{Q} = \rho\mathbf{v}$-pressure formulation).

The Stokes problem is discretized in space thanks to a finite element method. The unstructured meshes use triangles or tetrahedra with a mixed formulation for the velocity and the pressure in order to get a well posed Stokes problem. The elements available in the N3S code are P1-P2 or P1-isoP2 elements. In most industrial cases, we use the P1-isoP2 element. The velocity matrix can be mass-lumped without diminishing the global spatial precision. This leads to more simple calculations, especially in the case of varying density.

Effectively, the classical discretization of the generalized Stokes problem leads to unsymmetric problems which require specific algorithms. Another way consists in adding a fractional time step at time t^{n+1}: it is a predictor corrector type scheme (Chorin algorithm):[2]

$\tilde{\mathbf{v}}$ denotes the value obtained after the convection step, ρ^n density at time step t^n, $\mathbf{S}_v$ = source term for $\mathbf{v}^{n+1}$. μ denotes the viscosity of the fluid, μ_t, the eddy viscosity.

Velocity diffusion stage. We obtain an intermediate velocity field $\mathbf{v}^*$ by solving

$$\frac{\rho^n}{\Delta t}(\mathbf{v}^* - \tilde{\mathbf{v}}) - \nabla \cdot [(\mu + \mu_t)\nabla \mathbf{v}^*] + \nabla \rho^n = \mathbf{S}\mathbf{v} \tag{10}$$

Pressure continuity stage. It is applied to an increasing value of the pressure and thus, the final velocity $\mathbf{v}^{n+1}$ satisfies the continuity condition:

$$\begin{aligned} \frac{\rho^n}{\Delta t}\delta\mathbf{v} + \nabla \delta p &= 0 \\ -\nabla \cdot (\rho^n \delta \mathbf{v}) &= \nabla \cdot (\rho^n \mathbf{v}^*) \end{aligned} \tag{11}$$

where $\delta\rho = \rho^{n+1}$ and $\delta\mathbf{v} = \mathbf{v}^{n+1} - \mathbf{v}^*$. This system is unsymmetric. We introduce the momentum associated to $\delta\mathbf{v}$, defined by $\delta\mathbf{Q} = \rho^n \delta\mathbf{v}$. The system (11) can be replaced by

$$\begin{aligned} \frac{\delta\mathbf{Q}}{\Delta t} + \nabla \delta p &= 0 \\ -\nabla \cdot \delta\mathbf{Q} &= \nabla \cdot \mathbf{Q}^* \end{aligned} \tag{12}$$

The variational formulation of formula (12) leads to a symmetrical matricial system of the following type:

$$\begin{aligned} \mathbf{M}_Q \delta\mathbf{Q} + \mathbf{B}^t \delta p &= 0 \\ \mathbf{B}\delta\mathbf{Q} &= -\mathbf{B}\mathbf{Q}^* \end{aligned} \tag{13}$$

This system is solved by an iterative method of Uzawa type which is classical for elliptic problem with constraint type condition.

First $\delta\rho$ is calculated by elimination of $\delta\mathbf{Q}$ in (13):

$$\mathbf{B}\mathbf{M}_Q^{-1}\mathbf{B}^t\delta p = -\mathbf{B}\mathbf{Q}^* \tag{14}$$

and $\delta\mathbf{Q}$ is obtained *a posteriori*:

$$\delta\mathbf{Q} = -\mathbf{M}_Q^{-1}\mathbf{B}^t\delta p \tag{15}$$

To avoid to inverse a mass matrix as in (15), a mass-lumping technique is used. This is available only for the P1-isoP2 element and the calculation of $\mathbf{B}\mathbf{M}_Q^{-1}$ is reduced to a multiplication of a vector by a diagonal matrix.

In the case of constant density, this algorithm is naturally available.

3.5. *Projected gradient Uzawa algorithm*

$\Gamma_{\text{in},h}$, $\Gamma_{\text{out},h}$, $\Gamma_{\text{w},h}$ are portions of the boundary of the calculation domain Ω_h associated to Γ_{in}, Γ_{out}, Γ_{w} respectively. We consider in this section the P1-P2 triangle. We introduce discrete spaces:

$$X_h = \{\varphi \in C^0(\Omega_h)/\varphi \text{ is a 2nd -degree polynomial on each triangle}\}^N$$

$$M_h = \{q \in C^0(\Omega_h)/q \text{ is a 1st degree polynomial on each triangle}\} \cap L^2(\Omega_h)$$

$$V_{0,h} = \{\mathbf{w} \in X_h/\forall a \in \Gamma_{\text{in},h},\ \mathbf{w}(\mathbf{a}) = 0 \text{ and } \forall a \in \Gamma_{\text{w},h},\ \mathbf{w}(a)\mathbf{n}_h = 0\}$$

where $\mathbf{n}_h$ is a discrete normal vector.[13]

The discretized Stokes problem according to boundary conditions, as defined at Section 3.2 naturally uses test functions of $V_{0,h}$. Another way can be to solve the Stokes problem in a larger space (X_h) than $V_{0,h}$ and apply the boundary conditions thanks to a projection operator P_h from X_h onto $V_{0,h}$. For simplicity reasons, the algorithm is explained in the case where variational problem takes into account a constraint condition (as the pressure continuity step defined in Section 3.4). In other cases, the algorithm can be adapted easily.

We introduce the continuous bilinear form $a_h: X_h \times X_h \to \mathbf{R}$ related to the 'mass' discretized operator and $b_h: X_h \times M_h \to \mathbf{R}$ related to the 'divergence/gradient' discretized operator $l_h: X_h \to \mathbf{R}$ and $g_h: M_h \to \mathbf{R}$ are linear forms. They come from source terms and non-homogeneous Dirichlet conditions. The discretized pressure-continuity problem (12) is as follows:
Find $\delta\mathbf{q}_h \in X_h$, $\delta p_h \in M_h$ solutions of

$$a_h(P_h\delta\mathbf{q}_h, P_h\mathbf{w}) + b_h(P_h\mathbf{w}, \delta p_h) = l_h(P_h\mathbf{w}) \quad \forall \mathbf{w} \in X_h$$

$$b_h(P_h\delta\mathbf{q}_h, q) = g_h(q), \quad \forall q \in M_h$$

$$P_h\delta\mathbf{q}_h = \delta\mathbf{q}_h$$

P_h is symmetric. This leads to the linear system, where $\mathbf{A} = \mathbf{M}_Q$ for the pressure continuity system, is associated to a_h, $\mathbf{B}$ to b_h, L to l_h G to g_h: Find $\delta\mathbf{Q} \in X_h$, $p \in M_h$ solutions of

$$\mathbf{P}\mathbf{A}\mathbf{P}\delta\mathbf{Q} + \mathbf{P}\mathbf{B}^t\delta p = \mathbf{P}L$$

$$\mathbf{B}\mathbf{P}\delta\mathbf{Q} = G \tag{16}$$

$$\mathbf{P}\delta\mathbf{Q} = \delta\mathbf{Q}$$

The same technique as described in Section 3.4 (formulae (14) and (15)) is used to apply the projected gradient Uzawa algorithm to the problem with boundary conditions. The system can be easily solved thanks to the symmetry property of matrix $\mathbf{P}$.

3.6. Improvement of the code

An analysis of CPU time and memory requirement with the previous release of the code on a standard 3D industrial application leads to the following results:

(a) One important part of the time is needed for FE calculations and assembling of the different matrices (varying in time with the eddy viscosity) and r.h.s.; the main part of the out-of-core memory is used for storing all the FE information (containing, for each element and each Gauss point, basis function values, gradients, Jacobian matrix, elementary matrix).

(b) Another part of the CPU time is also used to solve large linear systems $\mathbf{Ax} = \mathbf{b}$, where $\mathbf{A}$ is a well-conditioned mass plus diffusion matrix (diffusion of all the variables such as velocity, temperature, k, ε), or where $\mathbf{A}$ is the Laplacian-like preconditioning matrix of the pressure system, equal to $\mathbf{BB}^{\mathrm{T}}$. We have then concentrated our efforts on optimizing these two points.

(i) *Elimination of FE file and optimization of FE calculation:*[10] Only triangle in 2-D and tetrahedron in 3-D are kept. These elements, named simplicial elements, have intresting properties which allow us to compute the elementary terms (matrix and r.h.s.) by hand. Based on this idea, we have developed a formal pre-processor adapted for all elementary matrix and r.h.s. calculations. For one type of matrix or r.h.s., all the elementary terms are then computed in a single loop whose length is the total number of elements (which is fully vectorized). Another consequence is the elimination of the FE file, and the decreasing of the access file time (or swapping time on workstation). The assembling of the elementary matrices in the global matrix is done with indirect addressing, so does not vectorize. We manage dependencies through FE reordering, and we can then force the vectorization on the computer.

(ii) *Optimization of the linear system solving:*[14] As we said, the linear systems are solved using an iterative Preconditioned Conjugate Gradient (PCG) algorithm, using matrices stored in a classical Symmetrical Compressed Row (SCR) structure. The efficiency of this algorithm is crucial (40 per cent of the total CPU time in a turbulent case up to 90 per cent in a laminar case, without including the computation of the matrices). Looking from a performance point of view, PCG calculation time is spent in three operations:

(1) direct solving of a linear system $\mathbf{C}z = r$, where $\mathbf{C}$ is the preconditioning of $\mathbf{A}$; the standard choice is the Incomplete Cholesky decomposition Preconditioning (ICP), which leads to the same SCR structure as $\mathbf{A}$ with the storage of the array AC(NCOEF); this step takes about 50 per cent of PCG CPU time;
(2) matrix-vector product, about 50 per cent of PCG CPU time;
(3) BLAS routines used (e.g. dot product, linear combination of vectors, scalar vector product), less than 5 per cent of PCG CPU time.

The main improvement consists in optimizing the matrix–vector product. With the classical SCR storage, this step is poorly vectorized: the length of the inner loop is half of the bandwidth, which depends on the connectivity of the mesh (say 5 in a 2-D case to 20 in a 3-D case with the quadratic elements used in N3S). To increase inner loop length, we changed to Jagged Diagonal (JD) storage. We only then replace the matrix–vector product by a much better vectorizable one (the size of the JD is the size of the system) plus a permutation, and the results and iterations are exactly the same if we do not change anything else. The speed-up obtained for just the matrix–vector product turns out to be 12 in 2-D and 6 in 3-D for all the test cases.

This part using less CPU time, we can replace the IC preconditioning (very bad vectorized) by a more simple one, like a Diagonal Preconditioning (DP). We will need more iterations, but each one is less expensive in time.

4. APPLICATION TO FLOWS IN HEATED ROOMS

The comfort notion in habitation is related to fluid dynamic parameters. The temperature gradients have to be as small as possible, the air currents indiscernible but strong enough to evacuate the pollutants. All these conditions are challenges to the conception of heating apparatus. The flows generated by heating or cooling systems are generally very complex and rise many difficulties to be modelled. Numerical methods seem to be useful to study the movements of air in habitations. Different complementary approaches are developed by EDF. For the first ones, the global models, each room is cut in few areas, the solver evaluates the heat and mass transfer from one area to another. Another approach consists in evaluating the ability of thermohydraulic codes like N3S to predict the thermal and dynamic characteristics of this kind of flows. Different heating systems have been simulated with N3S. The configurations correspond to an experimental set-up that was elaborated by EDF and the LET* in order to create flows similar to those in real habitations.

4.1. The experimental set-up

The set-up consists in a square cavity, in which small gaps have been arranged in walls to inject hot or cold air. The test cell is 300 mm wide, 1040 mm long and 1040 mm high. In order to generate two-dimensional flows,there are two other identical cavities on each side of the test cell. The heating systems that have been simulated are the convector,the heating floor and the heating

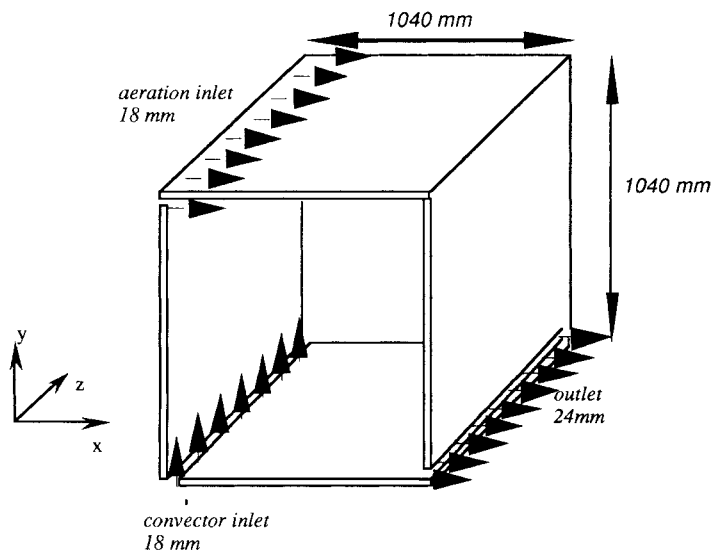

Figure 2. The experimental set-up

* Laboratoire d'Etudes Thermiques de Poitiers 40, avenue du Docteur Pineau 86022 Poitiers cedex.

ceiling. For each configuration, an external flow enters the enclosure through an opening (18 mm) in the top of the left vertical wall and exits from another opening (24 mm) located in the bottom of the right vertical wall. The convector is simply represented by an injection of hot air on the left end of the floor through a 18 mm gap (Figure 2). The mixed convection in the test cell was studied considering isothermal boundary conditions. All the walls are kept at fixed cold temperature, generally the same temperature as the aeration except the floor in the heating floor and heating ceiling configuration, the thermal source being then, respectively, the low horizontal wall and the high horizontal wall. The velocities can be chosen between 0 and 1 m/s. The temperature of the air varies between 10 and 40°C for the aeration and between 20 and 70°C for the convector. The temperature inside the cavity is evaluated from readings of thermocouples regularly arranged in the cell. Velocity measurements are made by Laser-Doppler velocimetry. Prior to the measurements and to the calculations, a succession of visualizations was made in different configurations. These experiments revealed that the flows are extremely sensitive to the boundary conditions. A small alteration on the incoming velocity or temperature can provide two absolutely different behaviours.

4.2. Experimental results

Isothermal experiments lead to a great vortex all over the cavity area turning clockwise: the jet from the aeration gap hits the right wall and falls. The same structure was found with thermal sources either in the heating floor or in the convector configuration; however, if there is an important temperature difference and small velocities, the buoyancy terms can deviate the aeration jet and make it fall along the left wall as it comes into the cavity, generating an anticlockwise vortex. Clearly these flows are ruled by inertia or buoyancy effects and mainly two parameters arise in this kind of problem: the Reynolds number and the Froude (Fr) number.

In the heating floor and heating ceiling configurations, there is only one incoming flow and the Froude number (or the Richardson number $Ri = 1/Fr^2$) is the only criterion. The Froude number is defined as

$$Fr = \frac{Va}{\sqrt{ge\beta\Delta T}}$$

where e is the width of the opening, ΔT the temperature difference between the aeration and the heating floor, g the magnitude of gravitational acceleration and β the coefficient of thermal expansion. In the case of the heating floor, it was observed that for Fr greater than 3·67 the flow is dominated by the inertia effects and turns clockwise and for Fr lower than 1·83 the flow is dominated by buoyancy effects and turns in the opposite direction (Figure 3(a)). An intermediate flow corresponding to a critical value of the Froude number was obtained for $Fr \approx 3{\cdot}23$, in which case the incoming flow is not strong enough to reach the right vertical wall and is deviated in the middle of the ceiling (Figure 3(b)).

In the case of the convector, the thermal source is hot jet that gives rise to perturbations that have to be taken into account. The same structures have been noticed, as far as the big vortices are concerned, when the flow is fully dominated either by buoyancy or inertia, but they cannot be classified in respect of only one criterion. Four cases are detailed in Table I. In the critical flow configuration, the cold air from aeration falls along the left wall and get mixed in the middle of the cavity with the up-coming hot air from the convector (Figure 3(b)).

For the heating ceiling as for the other heating systems, two categories of flows have been observed according to the Froude number value, but here the flow is a bit more difficult to characterize. The critical value of the Froude number is about $Fr_C = 3{\cdot}67$ For higher values, the

(a)

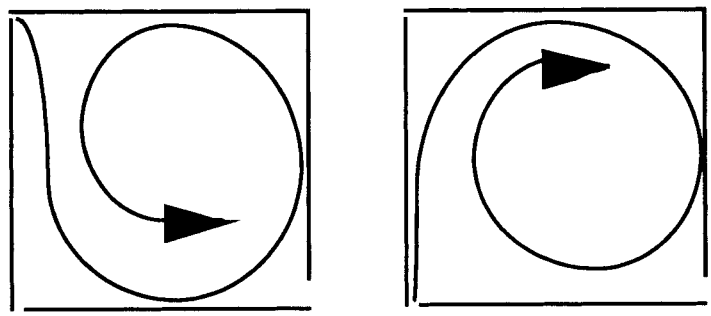

(b)

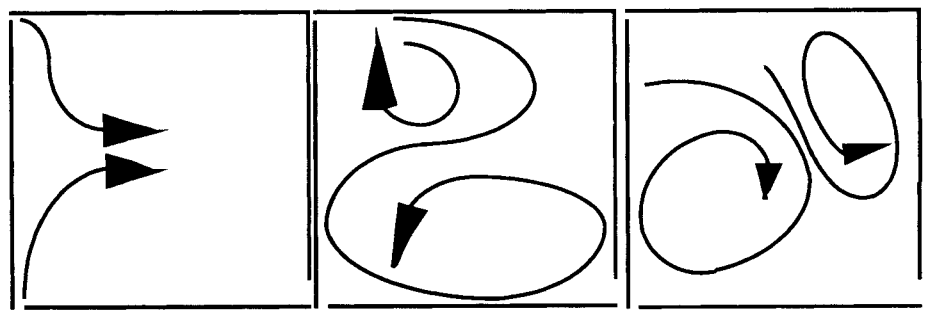

Figure 3. Flows structure: (a) stable flows dominated by inertia and buoyancy; (b) critical flows, respectively, for the convector, for the heating floor and for the heating ceiling

Table I. The dominating phenomena in the convector configuration for various parameters (Fr_a and Fr_c represent, respectively, the Froude numbers in the aeration and convector areas)

V_a	V_c	T_a	T_c	T_w	Fr_a	Fr_c	Flow dominated by
0·3	0·3	18·5	23·5	18·5	11·6	5·8	Inertia
0·3	0·3	13·0	63·0	40·0	2·5	2·3	Inertia
0·18	0·10	11·0	28·0	20·0	2·3	1·9	Buoyancy
0·15	0·15	13·0	63·0	40·0	1·2	1·1	Inertia

flow is dominated by inertia, but the pattern is no more a lonely vortex turning clockwise, as a matter of fact a smaller anticlockwise vortex appears in the lower left part of cavity. For the flow dominated by buoyancy effects ($Fr < 3{\cdot}67$), the aeration jet fall along the left wall, and a stratification appears in right part of cavity.

4.3. Calculations

All the flows generated are turbulent. Numerically, the turbulence effects are represented with the k–ε model and the heat transfer on walls is simulated by the modelling presented above. It can be expected that a pure natural convection problem requires a low-Reynolds model, but in each configuration studied here, the velocities of the air injected seem to be high enough to consider

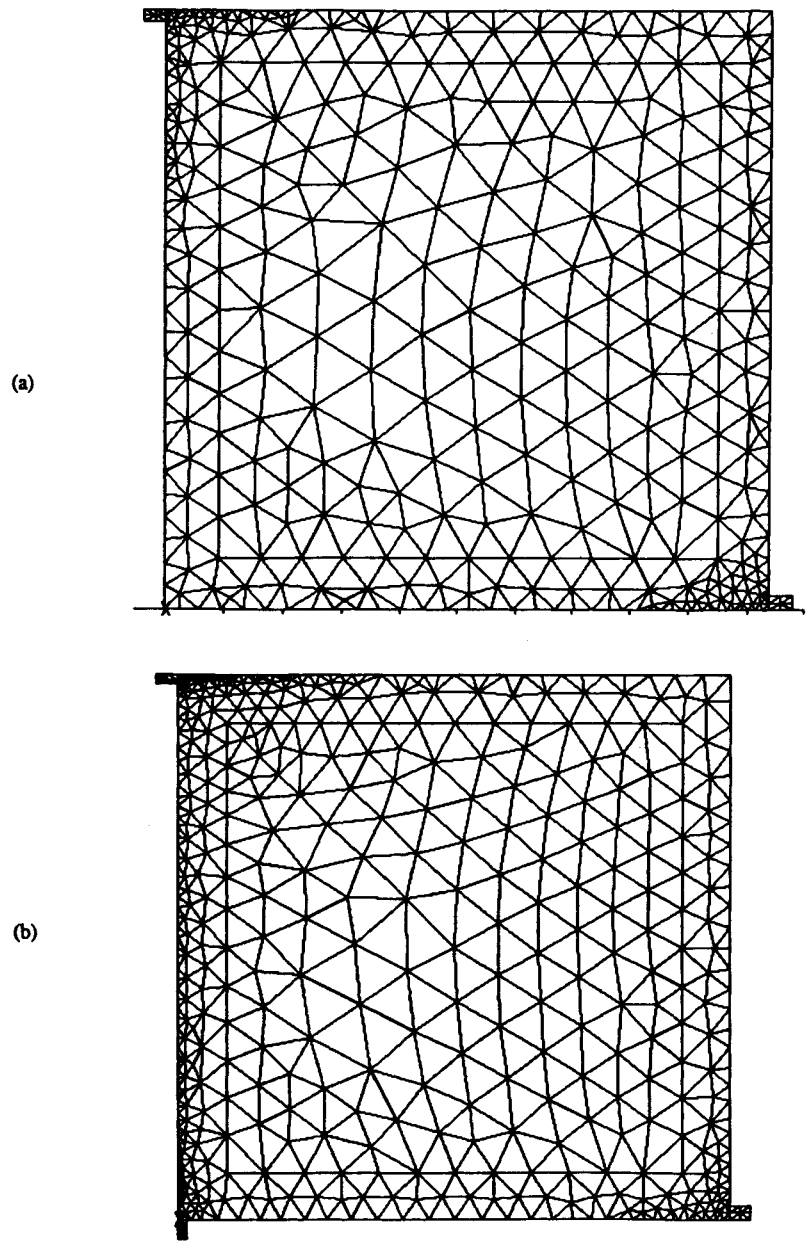

Figure 4. Grids used (a) in the heating floor and in the heating ceiling configuration; (b) in the convector configuration

that the heat transfer is due to mixed convection. In order to take into account the buoyancy effect, the Navier–Stokes equations are coupled to the energy equation through the Boussinesq approximation. One configuration of each heating apparatus has been computed.

The data for the heating floor are $V_a = 0{\cdot}57$ m/s, $T_a = T_w = 15°C$, $T_f = 35°C$; this leads to $Fr = 5{\cdot}19$. Actually, the flow generated experimentally is very stable, and the clockwise vortex occupies the whole cavity. As a result, the temperature field is very homogeneous between 19 and 20°C in the middle of the cell. For the numerical study, the grid used is made of 687 elements and 1526 nodes; it is reported in Figure 4. The elements are triangle P1-isoP2. The time step applied for this calculation is $dt = 0{\cdot}01$ s. 20 000 time steps have been computed during 1 h CPU time on Cray YMP (that corresponds to 0·1 s for 1000 nodes per time step). Velocities and turbulent parameters fields converge in less than 5000 iterations but the convergence of the temperature field is harder to reach, specially in the centre of the cell where all the velocities are very low.

The data for the heating ceiling are $V_a = 0{\cdot}57$ m/s, $T_a = T_w = 15°C$, $T_f = 35°C$; this leads to $Fr = 5{\cdot}19$. A clockwise vortex occupies the upper half of cavity, and a anticlockwise the other part. This flow is less stable than the last one. Furthermore, there are no measurements all over the cavity, they have been made along two profiles only. As a result, the temperature field is very homogeneous between 19 and 19·5°C in the middle of the cell. For the numerical study, the grid used is the same as the heating floor case (Figure 4). The elements are triangle P1-isoP2. The time step applied for this calculation is $dt = 0{\cdot}01$ s. 20 000 time steps have been computed during 1 h CPU time on Cray YMP (that corresponds to 0·1 s for 1000 nodes per time step). Velocities and turbulent parameters fields converge in less than 5000 iterations but the convergence of the temperature field is harder to reach, as in heating floor case.

The data for the convector are $V_a = 0{\cdot}6$ m/s, $V_c = 0{\cdot}2$ m/s, $T_a = T_w = 20°C$, $T_c = 40°C$. There is actually a big vortex occupying most of the cell, but there is also a very small one turning in the opposite direction just under the aeration opening. In this case, both buoyancy and inertia act on the flow structure, which corresponds to a critical flow. Near the aeration gap, the buoyancy effects are dominating and the cold air falls along the left wall. Then, lower, this air is submitted to the thrust of the up-coming hot jet and goes up again, creating the smaller vortex and deviating the hot jet to the right. Apart from this secondary vortex region and the regions close to the walls, the temperature in the main part of the cavity is one more time very homogeneous between 25 and 26°C. For the numerical study, a different mesh was used, made of 881 elements (triangle P1-isoP2) and 1952 nodes (Figure 4). The time step applied for this calculation is $dt = 0{\cdot}05$ s. 6000 time steps have been computed. The first iterations were computed neglecting the buoyancy terms in order to create a proper initial state before taking into account the buoyancy terms through the Boussinesq approximation.

4.4. Numerical results

In the heating floor case, the numerical results are in good agreement with the experimentation. N3S simulates a big vortex occupying all the cavity. The calculated velocities near the walls are a bit more important than the measured ones as can be seen on velocities distributions. (Figure 5). In the middle of the cell the temperature is too small for about 0·5°C compared to the measurements. Near the walls, the same deviation is noticed (Figure 6).

The temperature still progresses after 6000 time steps although the velocity field is absolutely converged.

The last 14 000 iterations raised the temperature in the middle of the cell by 0·5°C only, without any consequence on the dynamic parameters.

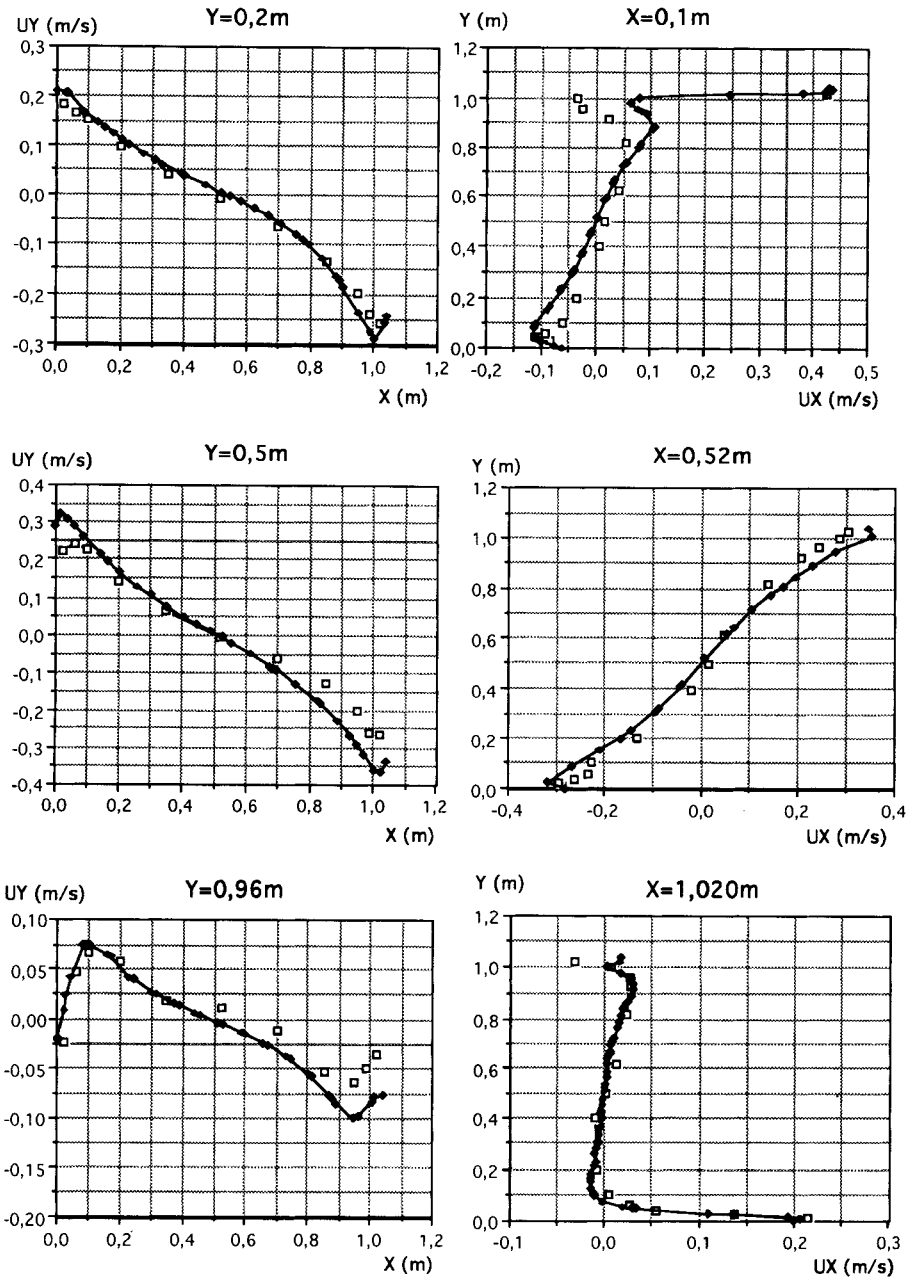

Figure 5. Vertical (UY) and horizontal (UX) velocity profiles in the heating floor configuration: (□) measurements; (—◆—) calculation

For the heating ceiling configuration, the lack of experimental data prevents us from doing significant comparisons. N3S simulates two vortex, one turning clockwise in the upper half part of cavity and an anticlockwise vortex in the lower part. As in the heating floor case, the velocity field and the temperature gradients are well described (Figures 7 and 8). The temperature is

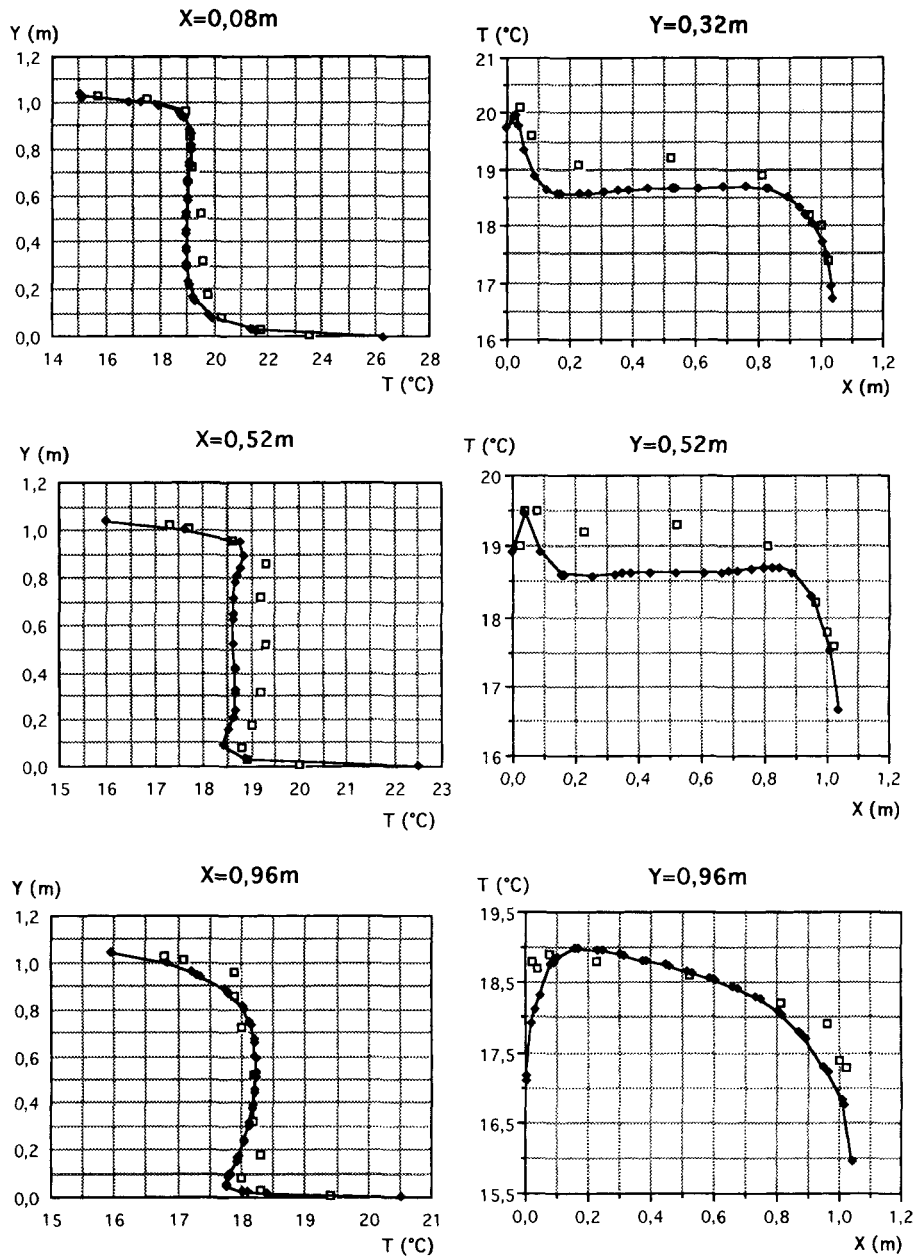

Figure 6. Temperature profiles in the heating floor configuration: (□) measurements; (—◆—) calculation

simulated with slightly less accuracy with a deviation of 1·5°C in the middle of the room and near the walls; This typical configuration is more unstable, so really difficult to simulate. The time steps for converence are similar to the heating floor case.

The simulation of the convector gave rise to a lonely vortex turning clockwise and occupying all the cavity. According to the numerical results, the buoyancy effects are not strong enough to

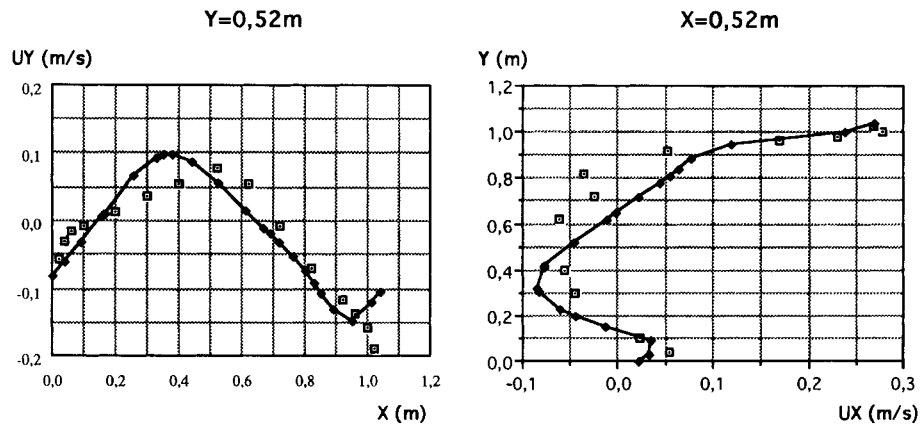

Figure 7. Vertical (UY) and horizontal (UX) velocity profiles in the heating ceiling configuration: (□) measurements; (—◆—) calculation

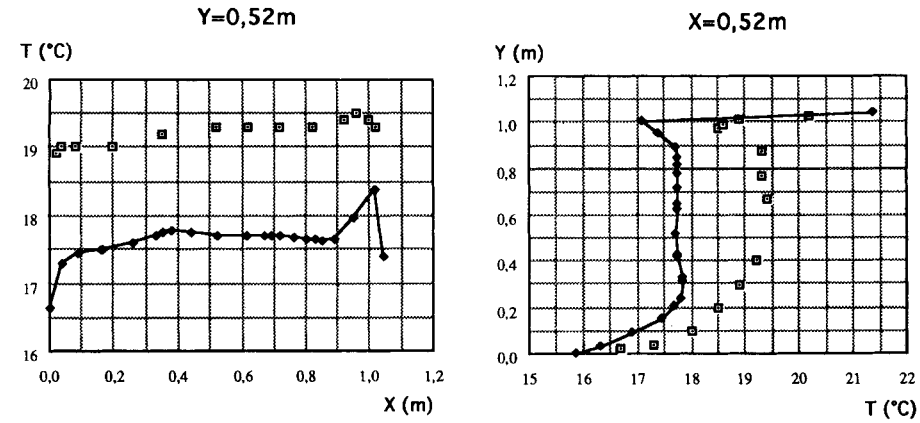

Figure 8. Temperature profiles in the heating ceiling configuration: (□) measurements; (—◆—) calculation

generate the secondary vortex under the aeration opening. The cold air entering the cell keeps an horizontal direction. This inaccuracy generates many other discrepancies that appear on the velocities profiles (Figure 9). The hot jet is not slowed down any more by the down-coming cold air. N3S simulates the jet all along the left wall although the experiment founds negative velocities in the top of this wall. Entering the cavity, the cold air is mixed to the vortex; this generates all along the edges of the cell too large velocities.

The temperature found by N3S in the core of the cavity is higher than the ones revealed by the measurements by a bit less than 1°C (Figure 10).

These three calculations reveal that the numerical solution does not detect the transition. However, in a stable configuration, the calculations provide very satisfying results although some discrepancies could be observed near the walls. This phenomenon appeared for the three

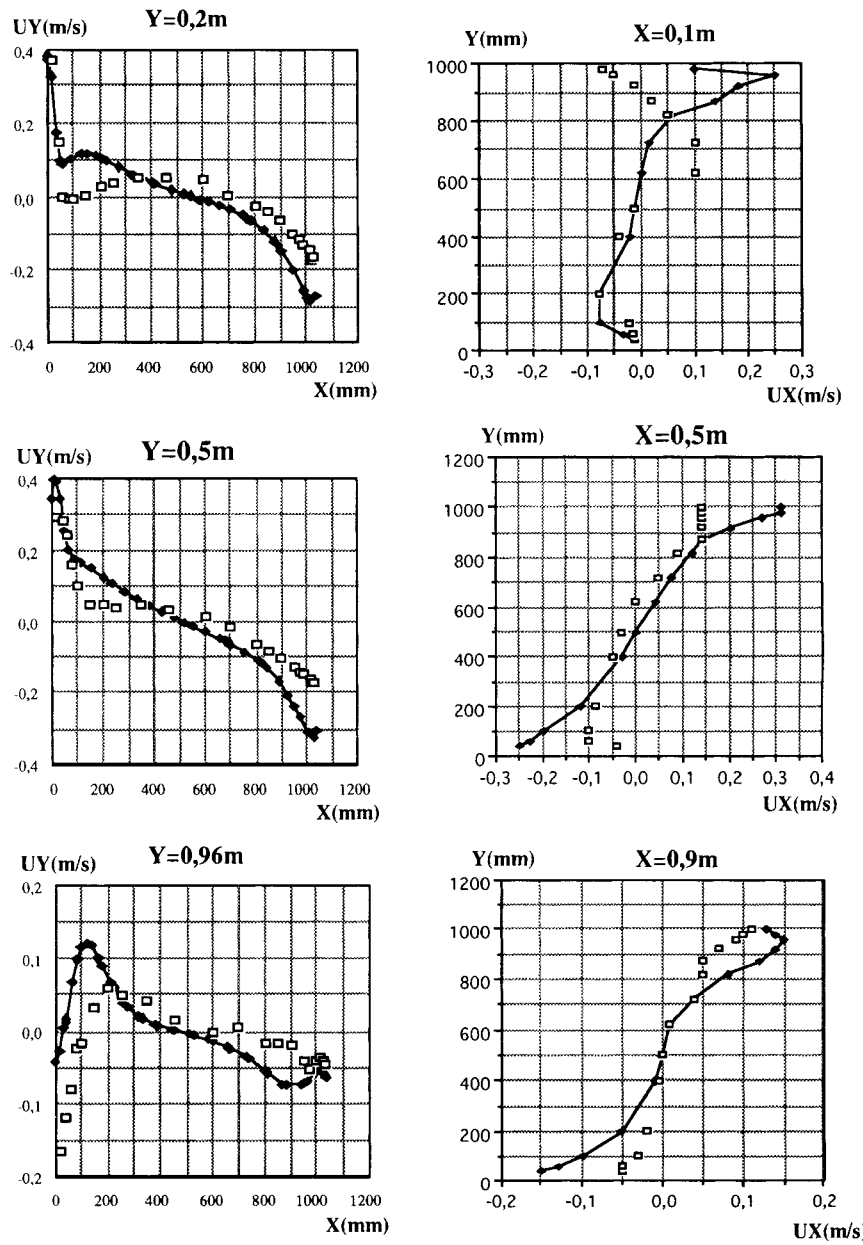

Figure 9. Vertical (UY) and horizontal (UX) velocity profiles in the convector configuration: (□) measurements; (—◆—) calculation

simulations so the code seems to underestimate the shear stress. This can be related to the fact that for this kind of flows, the viscous sublayer might be very thick, and the boundary layer modelling was designed for fully turbulent flows where the molecular viscosity interferes on very small length scales.

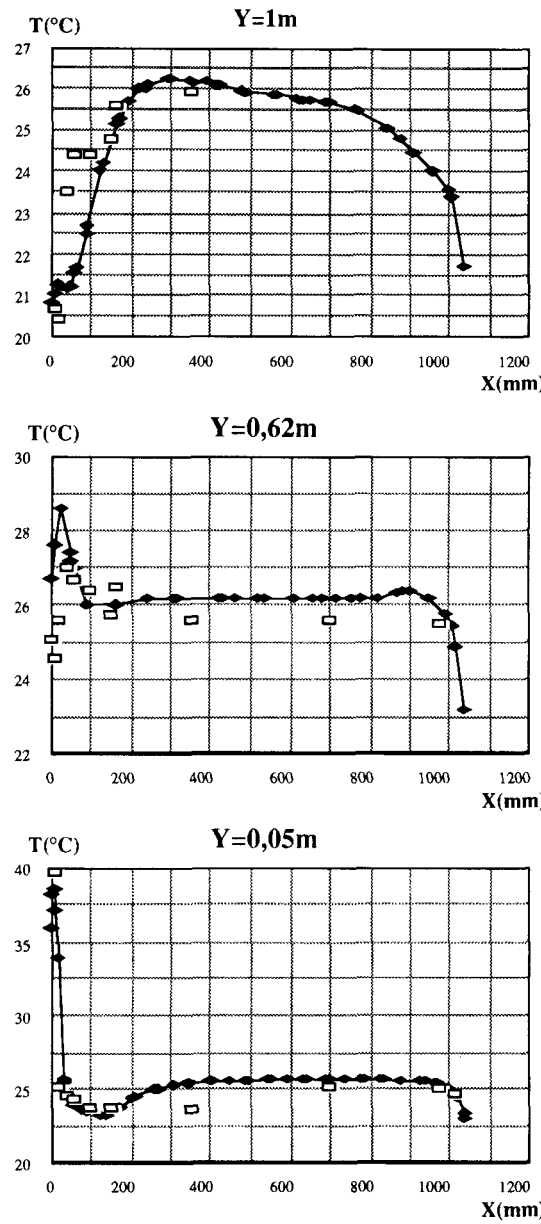

Figure 10. Temperature profiles in the convector configuration: (□) measurements; (—◆—) calculation

5. APPLICATION TO FLOWS IN COOLED ROOMS

This study presents a typical configuration of flow of mixed convection characterizing an air-conditioner encountered in habitations. As a matter of fact, the aerothermal phenomena in a cooled and ventilated room is very complex, and the actual cooling systems raise some

problems of comfort and efficiency. Thermohydraulic codes like N3S are able to constitute a solid base for the conception of such systems and to improve the understanding of aerothermal phenomena in buildings. Consequently, a validation of N3S is necessary to confirm the accuracy of simulation compared to the experimental data. The experimental measurements have been performed by the LET.

5.1. The experimental set-up

The set-up consists in a square cavity, in which small gaps have been arranged in walls to inject and extract air (Figure 11). The size of the cell is similar to the previous experiments. In a cooled

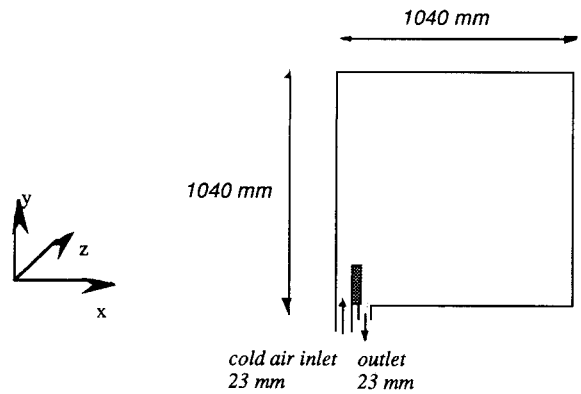

Figure 11. Experimental set-up of an air-conditioner

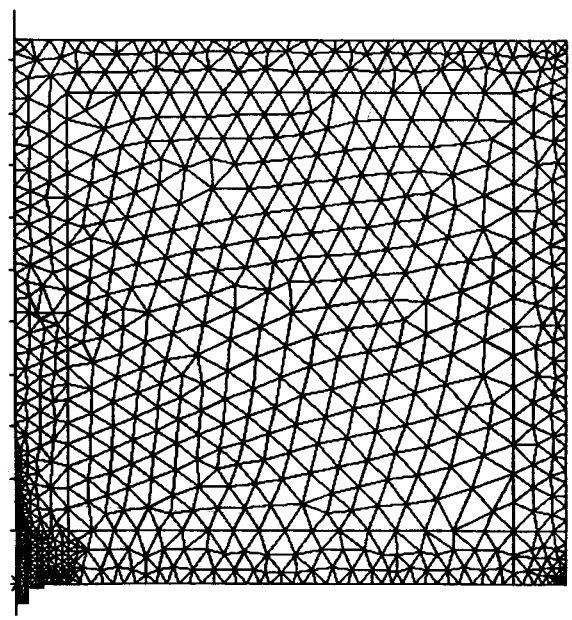

Figure 12. Grid used in the air-conditioner configuration

room, the intake of cold air is located at the corner of the left wall and the floor, through a gap of 23 mm. The extract of air is located near the entrance through a gap of 23 mm. Between the two gaps laid a vertical wall (4 mm width and 10 cm height). The air-conditioner thus is simply represented by an injection of cold air: $T_j = 17°C$. All the walls are kept at fixed temperature: $T_w = 26{\cdot}7°C$. The inlet velocity is chosen on an average at $U_j = 0{\cdot}73$ m/s. This leads to $Fr = 8{\cdot}5$.

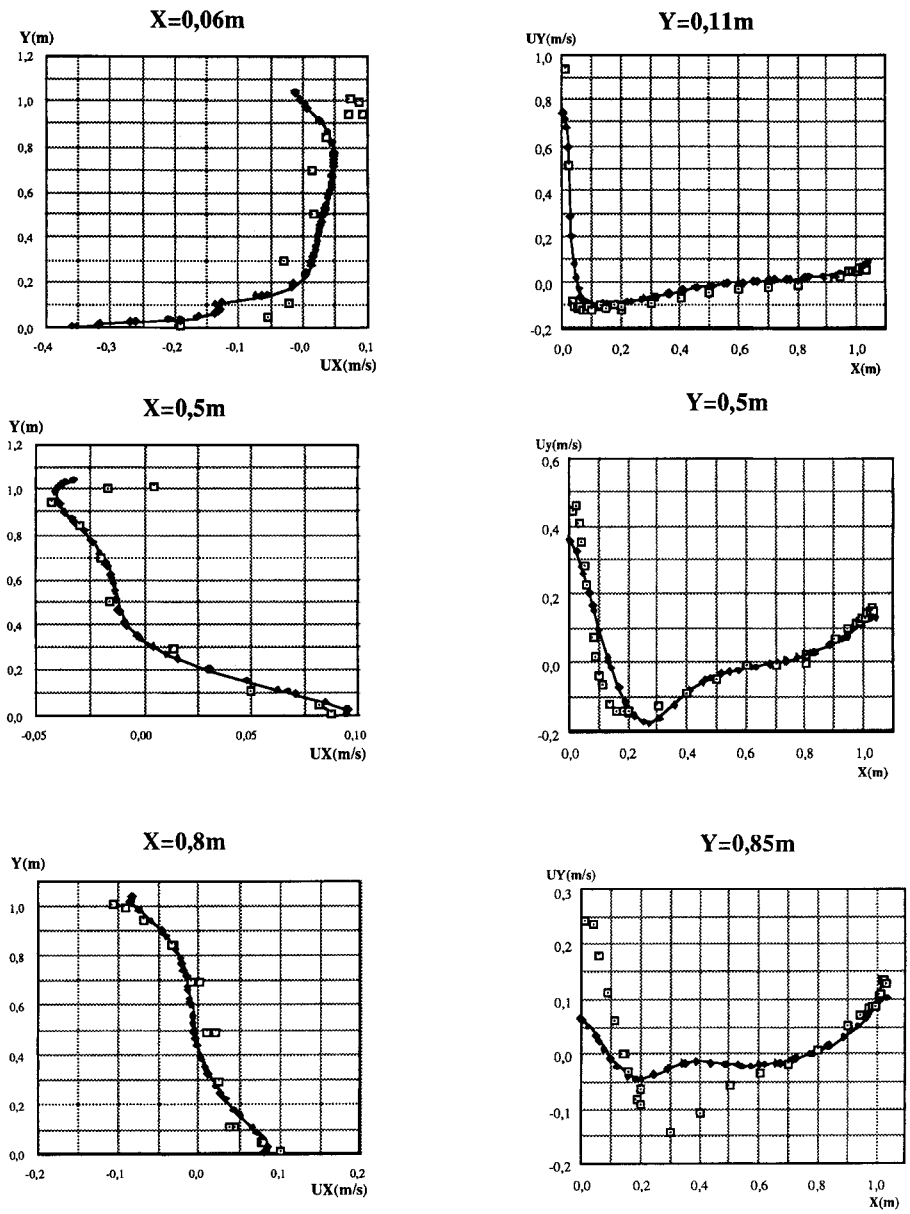

Figure 13. Vertical (UY) and horizontal (UX) velocity profiles in the air-conditioner configuration: (□) measurements; (—◆—) calculation

5.2. *Experimental results*

A plume of cold air is released from the inlet. The cold air makes its way to the ceiling and falls down in the left part of cavity, generating a clockwise vortex. In the right part of cell, the buoyancy and viscous terms induce an anticlockwise vortex. As in heating systems, the Froude

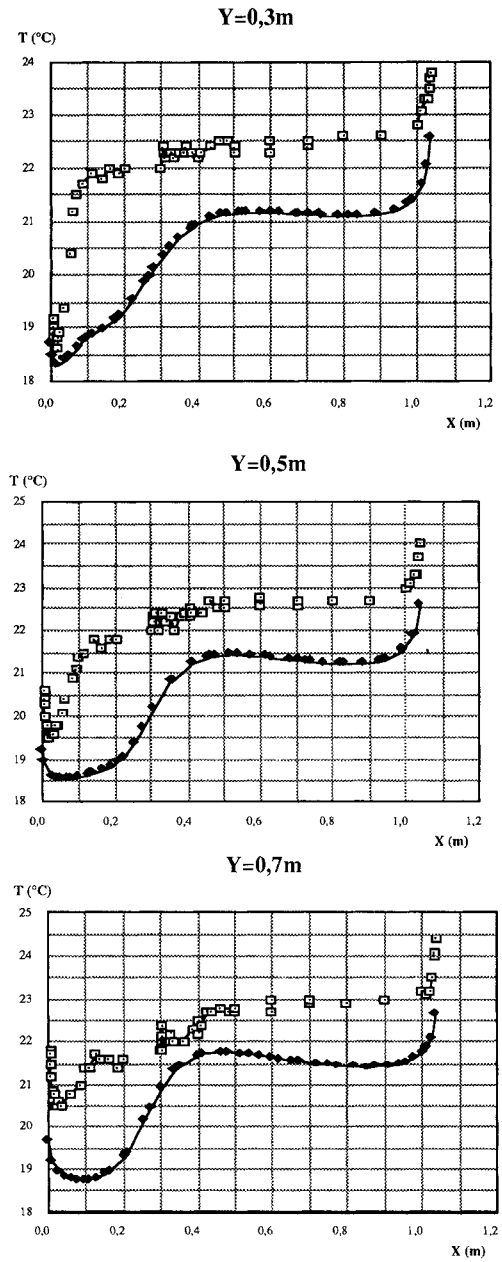

Figure 14. Temperature profiles in the air-conditioner configuration: (□) measurements; (—◆—) calculation

number is a determinant parameter for the aerothermal flow. The height of the plume depends only on the Froude number.

5.3. *Calculations*

The turbulent effects are represented with the standard k–ε model, and the buoyancy effects are taken into account with a variable density. The numerical data are similar to the experimental ones: $T_i = 17°C$, $T_w = 26{\cdot}7°C$ and $U_j = 0{\cdot}73$ m/s.

For the numerical study, the grid used is made of 1557 elements and 3342 nodes; it is reported on Figure 12. The elements are triangle P1-iso P2. The requested computation time is around 3000 s representing 5000 iterations of 0·1 s of real time, that is to say 0·18 s for 1000 nodes and by time step.

The permanent state is obtained by using a transient integration. The convergence period thus corresponds to the data spreading over the whole field. Temperature and velocities parameters converge in less than 4000 iterations.

5.4. *Numerical results*

In terms of accuracy, the velocity field is well described on the whole cavity. N3S simulates a plume on the left part of the cell a little lower and wider than the experimental one. Some other simulations have confirmed that the velocity profile of the injected air has little consequence on the plume size. On the right part, the anticlockwise vortex, is in good agreement with the experimentation. The temperature field is simulated with slightly less accuracy: An under-assessment of 1·5°C have been recorded in the centre of cavity.

N3S matches the velocity field analysis particularly well (Figure 13), but matches to a lesser degree that of thermal exchanges (Figure 14). This conclusion confirms the first results from the simulation of aerothermal phenomena in a heated and ventilated room.

6. CONCLUSION

Flows generated by heating or cooling apparatus have been simulated with the finite element code N3S. The calculations presented here concern the simulation of aerothermal phenomena in a heated or a cooled ventilated room. On a qualitative point of view the numerical results are in good agreement with the measurements although some differences could be pointed out in unstable configurations. The wall law model for the thermal boundary layer presented seems to be able to simulate the heat transfer in mixed convection flows in enclosures, but clearly, in order to compute pure natural convection problems, a low-Reynolds model is required as the temperature profile is not logarithmic in such cases. Considering the applications presented here, it can be expected that this modelling can provide satisfactory informations for any industrial application in three dimensions. Along the same line, some more works are under way, it consists in implementing in the code a second moment closure, more realistic than the k–ε model to represent the turbulent effects, the development of adaptative meshing procedures may also improve the accuracy of the solution.

NOTATION

$a, a_t, a_e^+ = (a + a_t)/v$ molecular, turbulent and equivalent diffusivity

C_p specific heat at constant pressure

l_m mixing length
q_w heat flux from wall to fluid
$T^+ = (T - T_w)/T^*$ dimensionless temperature
$T^* = q_w/\rho Cpu^*$ friction temperature
T_a, T_c air temperatures from aeration and from convector
T_f, T_w temperature of the floor and of the other walls
u^* friction velocity
V_a, V_c velocity of the air from aeration and convector
$y^* = yu^*/v$ dimensionless distance to the wall
v, v_t kinetic molecular and turbulent viscosity
ρ density

REFERENCES

1. J.-P. Chabard, B. Métivet, G. Pot and B. Thomas, 'An efficient finite element method for the computation of 3D turbulent incompressible flows, *Finite Elements in Fluids*, **8,** 239–293, 1992.
2. A. Caruso and N. Méchitoua, 'Finite element computations of turbulent diffusion flame', *Proc. 2nd Int. Conf. in Advanced Computational Methods in Heat Transfer*, Milan, Italy, July 1992.
3. J.-P. Chabard, B. Delenne, G. Pot and E. Razafindrakoto, 'Application of N3S code to the computation of an axisymetric jet impinging a flat plate', *15th Meeting of the A.I.H.R. Working Group on Refined Modelling*, Lyon, France, October 1991.
4. J.-F. Combes, I. Grimbert and E. Rieutord, 'An analysis of the viscous flow in a centrifugal pump with a finite element code', *Proc. Fluid Machinery Forum*, Portland, OR, June 1991.
5. C. Patel, W. Rodi and G. Scheuerer, 'Turbulence models for near wall and low Reynolds Number flows: A review', *AIAA J.*, **23**(9), 1308–1319 (1985).
6. E. R. Van driest, 'On turbulent flow near a wall', *J. Aeronaut. Sci.*, **23,** 1007 (1956).
7. B. A. Kader and M. Yaglom, 'Heat and mass transfer laws for fully turbulent walls flows', *J. Heat Mass Transfer*, **15,** 2329 (1972).
8. B. A. Kader, 'Temperature and concentration profiles in fully turbulent boundary layers', *J. Heat Mass Transfer*, **24,** 1541 (1981).
9. V. Arpaci and P. Larsen, *Convective Heat Transfer*, Prentice Hall, Englewood Cliffs, N.J., 1984.
10. G. Pot, O. Bonnin, V. Moulin and B. Thomas, 'Improvement of finite element algorithms implemented in CFD code N3S for industrial turbulent applications,' *Proc. 8th Int. Conf. on Numerical Methods in Laminar and Turbulent flow*, Swansea, U.K., July 1993.
11. K. Boukir, Y. Maday and B. Métivet, 'A high order characteristics method for the incompressible Navier–Stokes equations', *Proc. Int. Conf. on Spectral and High Order Methods*, Montpellier, France, June 1992.
12. C. Bernardi, F. Laval, B. Métivet and B. Thomas, 'Finite element approximation of viscous flows with varying density', *SIAM J. Numer. Anal.*, **29**(5), 1203–1243 (1992).
13. M. S. Engelman, R. L. Sani and P. M. Gresho, 'The implementation of normal and tangential velocity boundary conditions in finite element codes for incompressible fluid flow', *Int. j. numer. methods fluids*, **2,** 225–238 (1982).
14. G. Pot, J. P. Grégoire and B. Nitrosso, 'Conjugate gradient's performances enhanced in the C.F.D. code N3S by using a better vectorization of matrix vector product', *Proc. IMAC'S 91*, Dublin, Ireland, July 1991.